

Current-Crowding-Free Superconducting Nanowire Single-Photon Detectors

Stefan Strohauer,^{1,2,*} Fabian Wietschorke,^{1,3} Christian Schmid,^{1,3} Stefanie Grotowski,^{1,2}
Lucio Zugliani,^{1,3} Björn Jonas,^{1,3} Kai Müller,^{1,3,4} and Jonathan J. Finley^{1,2,4,†}

¹Walter Schottky Institute, Technical University of Munich, 85748 Garching, Germany

²TUM School of Natural Sciences, Technical University of Munich, 85748 Garching, Germany

³TUM School of Computation, Information and Technology,
Technical University of Munich, 80333 Munich, Germany

⁴Munich Center for Quantum Science and Technology (MCQST), 80799 Munich, Germany

(Dated: July 18, 2024)

Detecting single photons is essential for applications such as dark matter detection, quantum science and technology, and biomedical imaging. Superconducting nanowire single-photon detectors (SNSPDs) excel in this task due to their near-unity detection efficiency, sub-Hz dark count rates, and picosecond timing jitter. However, a local increase of current density (current crowding) in the bends of meander-shaped SNSPDs limits these performance metrics. By locally irradiating the straight segments of SNSPDs with helium ions while leaving the bends unirradiated, we realize current-crowding-free SNSPDs with simultaneously enhanced sensitivity: after irradiation with 800 ions nm⁻², locally irradiated SNSPDs showed a relative saturation plateau width of 37% while fully irradiated SNSPDs reached only 10%. This larger relative plateau width allows operation at lower relative bias currents, thereby reducing the dark count rate while still detecting single photons efficiently. We achieve an internal detection efficiency of 94% for a wavelength of 780 nm with a dark count rate of 7 mHz near the onset of saturating detection efficiency.

Superconducting nanowire single-photon detectors (SNSPDs) [1] are widely used across fields such as quantum science and technology [2–9], astronomy [10], optical communication [11, 12], biology [13, 14], and medicine [15]. Their ability to detect single photons with near-unity efficiency [16, 17], sub-Hz dark count rate [18], picosecond timing jitter [19], and nanosecond reset time [20] makes them ideally suited for demanding applications such as photonic quantum computing [21–27], particle and dark matter detection [28–31], or infrared fluorescence microscopy for in vivo deep brain imaging [13, 14]. One strategy to further enhance detection efficiency, dark count rate, and timing jitter of SNSPDs is to reduce the effect of current crowding in their bends. Current crowding locally increases the current density in the bends, limiting the maximum applicable bias current through the detector, and thus limiting also the maximum achievable detection efficiency, dark count rate, and timing jitter [32, 33]. In literature, methods to reduce the effect of current crowding consist of optimized bend geometries [32–36], or increased superconductor thickness in the bends [37, 38]. The use of optimized bend geometries is either limited to relatively low-fill factor SNSPDs, which have lower absorption and detection efficiency, or requires a spiral or special meander design with significant wire length overhead, which is incompatible with dense SNSPD arrays and limits the timing properties of the detector. In contrast, variable thickness SNSPDs successfully reduce current crowding also for highly efficient and compact large fill factor SNSPDs. In this work, we introduce a novel method to obtain not only current-

crowding-free SNSPDs of arbitrary geometry and fill factor but also to simultaneously enhance their sensitivity.

I. CURRENT CROWDING AT LOW TEMPERATURES

Current crowding describes a non-uniform distribution of current density in an electrical conductor and has its origin for example in variations in material properties or device geometry. In the context of SNSPDs, current crowding leads to a local increase of the supercurrent density in the 180° bends and at kinks or discontinuities of the SNSPD. Once this current density exceeds the critical value for the superconductor, the SNSPD switches to the normal conducting state. This maximum current defines the switching current I_{sw} . In other words, current crowding limits I_{sw} of the SNSPD.

It is worthwhile to note that the effect of current crowding is most pronounced at low temperatures ($< 0.7T_c$), while at temperatures close to T_c the switching current practically coincides for straight and bent wires due to the divergence of the coherence length at temperatures close to the critical temperature [39, 40]. To quantify the effect of current crowding for our devices, we measured the temperature dependence of the switching current for SNSPDs (in meander form with 180° bends) and straight wires (without any bend), both consisting of 250 nm wide and 8 nm thick NbTiN wires. As shown for two representative devices in Figure 1, the switching current increases and the effect of current crowding becomes more prominent towards low temperatures, reaching a saturating (relative) difference between I_{sw} of the straight wire and the SNSPD at temperatures below 1.6 K (1 K). In fact, at temperatures below 1 K, the

* stefan.strohauer@tum.de

† jj.finley@tum.de

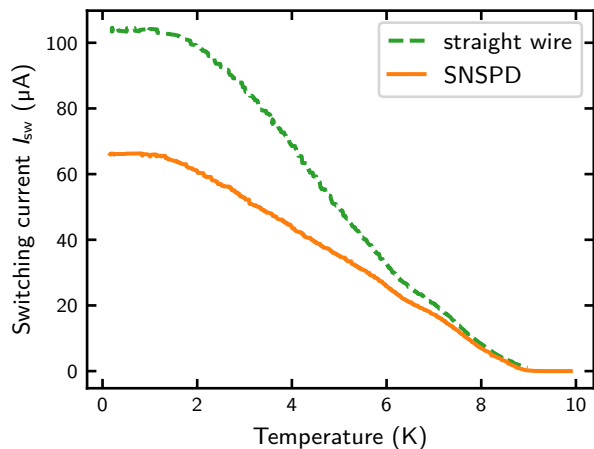


FIG. 1. Switching current versus temperature for an SNSPD and a straight wire. Current crowding causes a reduced switching current for the SNSPD over the straight wire, especially towards low temperatures.

switching current of NbTiN meander SNSPDs with a fill factor of 71 % and 250 nm wide wires is reduced to only 60 % of I_{sw} of corresponding straight wires.

At the same time, a high switching current, as close as possible to the limit set by the depairing current density, is desirable because it allows larger plateaus of saturating detection efficiency [19, 41]. This makes operation with high detection efficiency at simultaneously low dark count rates possible. Moreover, high switching currents allow high bias currents through the SNSPDs that yield high and easily detectable voltage pulses and low timing jitter [38]. Since high switching currents are reached for low temperatures where current crowding limits the maximum applicable bias current, a method to avoid current crowding would be highly advantageous. Moreover, current-crowding-free SNSPDs are expected to exhibit fewer dark counts since they originate primarily from bends or constrictions with strong current crowding [34, 37, 42–44]. Compared to methods presented in literature that solely mitigate current crowding [32–38], the following section introduces a solution to obtain current-crowding-free SNSPDs of arbitrary geometry that simultaneously exhibit enhanced sensitivity.

II. DESIGN AND CONCEPT OF CURRENT-CROWDING-FREE SNSPDs WITH ENHANCED SENSITIVITY

To demonstrate current-crowding-free SNSPDs of enhanced sensitivity, we combine the two effects of reduced switching current and enhanced sensitivity of SNSPDs after helium (He) ion irradiation [45, 46]. As discussed in the previous section, the 180° bends are the main contribution to current crowding in a meander-type SNSPD, thus limiting its switching current. By locally irradiat-

ing only the straight segments of the SNSPD while leaving its bends unirradiated, we reduce the critical current density of the straight segments while making them simultaneously more sensitive to single photons. Once the He ion fluence is large enough, the critical current of the straight segments with homogeneous current density will be lower than the critical current of the bends. Then, one can expect the overall critical current (or switching current) of the SNSPD to be given by the critical current of the straight segments and not being limited by current crowding anymore. To investigate this hypothesis, three types of devices as shown in Figure 2a were fabricated on the same chip: SNSPDs that were *locally* (only their straight segments) or *fully* irradiated, as well as *straight wires* without any bend. They were fabricated from an 8 nm thick NbTiN film on a Si substrate with 130 nm thermally grown SiO₂. The nominal design of the detectors consists of 250 nm wide nanowires in meander form with 100 nm gaps (fill factor 71 %) and covers an active area of 20 μ m \times 20 μ m. This high fill factor, along with the nominally rectangular design of the bends between neighboring nanowires, was chosen to have a pronounced effect of current crowding. The reference straight wires were fabricated on the same chip, also with a wire width of 250 nm. All devices were characterized prior to irradiation by measuring their switching current distributions and mean switching currents at a temperature of 1 K. After characterization of the unirradiated devices, a He ion microscope (Zeiss Orion Nanofab) with an acceleration voltage of 30 kV was used to irradiate them with He ions. An irradiation area of 25 μ m \times 15 μ m was centered on the 20 μ m \times 20 μ m detectors to homogeneously expose the straight segments of the nanowires while leaving the bends unirradiated. In this way, locally irradiated SNSPDs as shown in Figures 2a and 2b were obtained. For the reference straight wires, an irradiation area of 5 μ m \times 15 μ m was chosen. Moreover, two detectors were fully irradiated (25 μ m \times 25 μ m irradiation area). After irradiation, the devices were characterized again, and for several devices the process of irradiation and subsequent measurement was repeated multiple times.

III. REDUCING CURRENT CROWDING BY LOCAL HE ION IRRADIATION

As shown in Figures 2c and 2d, the mean switching current of locally irradiated SNSPDs stays constant for doses up to (90 ± 20) ions nm⁻², while it continuously decreases for fully irradiated SNSPDs and straight wires. As anticipated, locally irradiated SNSPDs exhibit a constant I_{sw} until the He ion fluence reaches a level that reduces I_{sw} of the straight wires to comparable values. Beyond this point, I_{sw} of locally irradiated SNSPDs and straight wires follow a similar curve. The slightly smaller I_{sw} of locally irradiated SNSPDs compared to that of the straight wires can be attributed to the higher likelihood of imperfections in one of the many straight segments of

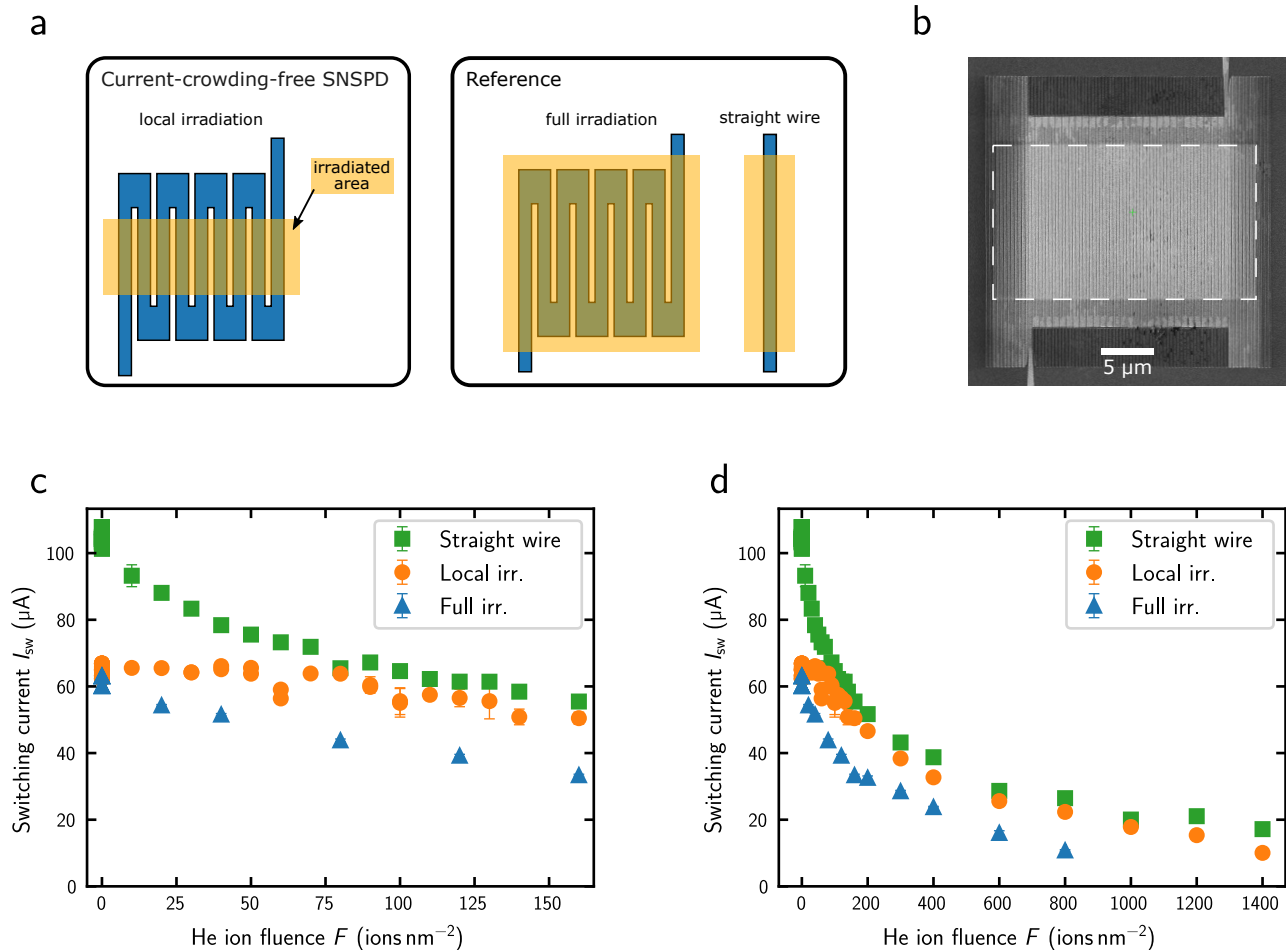


FIG. 2. Current-crowding-free SNSPDs. **a**, Local irradiation of the straight detector segments is used to obtain current-crowding-free SNSPDs. Fully irradiated SNSPDs and straight wires were fabricated as reference devices. **b**, Scanning electron microscope image of an SNSPD after local irradiation. The irradiation area is indicated by the white dashed rectangle. **c**, **d**, Switching current versus He ion fluence for *locally* as well as *fully* irradiated SNSPDs and straight wires for the low fluence regime (**c**) and for the full measured range up a fluence of 1400 ions nm⁻² (**d**).

an SNSPD, unlike in a single straight wire.

Figure 3 shows the temperature dependence of the maximum switching current for differently irradiated SNSPDs and straight wires, determined from the underlying switching current distributions [40, 47]. The critical temperature decreases continuously with increasing He ion fluence in accordance with literature [45, 46] and does not depend on device type or irradiation type. For decreasing temperature, the $I_{sw}(T)$ curves start to differ and show a smaller slope for fully irradiated SNSPDs compared to that of locally irradiated SNSPDs and irradiated straight wires. Moreover, for similar He ion fluences and low temperatures, I_{sw} is much smaller for fully irradiated SNSPDs than for locally irradiated SNSPDs or straight wires. For example, at temperatures below 1 K and for a He ion fluence of 300 ions nm⁻² it is only 30 μA instead of 40 μA. While for a He ion fluence of 60 ions nm⁻² the switching current of the straight wire

is still higher than that of the locally irradiated SNSPD, they almost coincide for the two fluences 110 ions nm⁻² and 130 ions nm⁻². Those observations support the hypothesis that for small He ion fluences I_{sw} of the locally irradiated SNSPDs is not reduced, while it starts to coincide with that of the straight wires for fluences above (90 ± 20) ions nm⁻². In this case, the irradiation induced reduction of the switching current in the straight segments is the limiting factor for I_{sw} instead of current crowding in the bends. The stronger the effect of current crowding in the unirradiated device, the higher the He ion fluence required for local irradiation such that current crowding no longer plays a role. Since current crowding limits the switching current of SNSPDs more as the fill factor increases, this method is particularly useful for high fill factor or micro-scale SNSPDs, especially if the detector requires He ion irradiation anyway to become single-photon sensitive [48, 49].

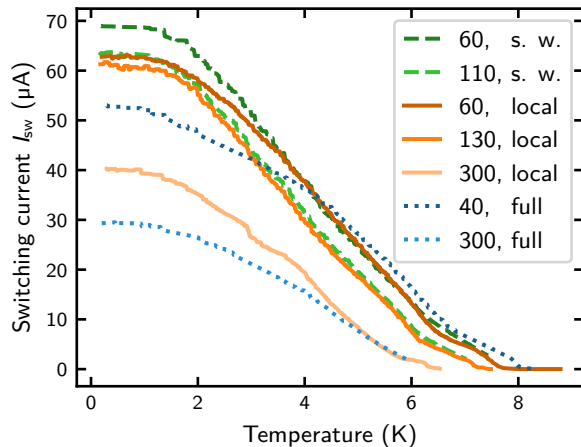


FIG. 3. Switching current I_{sw} of straight wires (s. w.), locally irradiated SNSPDs (local), and fully irradiated SNSPDs (full) versus temperature. The He ion fluence used for irradiation is given by the numbers in front of the device type in units of ions nm^{-2} .

IV. ENHANCED SENSITIVITY OF CURRENT-CROWDING-FREE SNSPDs

Helium ion irradiation enhances the sensitivity of SNSPDs. However, since we do not irradiate the whole SNSPD but intentionally leave the bends unirradiated and, consequently, do not have the irradiation induced decrease of switching current, we expect an enhanced performance due to two effects: (1) the He ion irradiation induced higher sensitivity, and (2) the higher available bias currents compared to fully irradiated SNSPDs of the same He ion fluence. Figure 4a shows a comparison of the normalized count rates between two devices, one irradiated locally and one irradiated fully, both with the same He ion fluences and for photons of 780 nm wavelength. The locally irradiated SNSPD clearly shows higher switching currents and larger saturation plateaus of the count rates, for which the internal detection efficiency is unity. Moreover, since the dark count rate at a certain bias current I_b mainly depends exponentially on the ratio I_b/I_{sw} , the dark count rate of locally irradiated SNSPDs is lower than that of fully irradiated SNSPDs at similar absolute bias currents or normalized count rates. Since our SNSPDs exhibit very low dark count rates, we measured it over an extended period of time for selected devices. As shown in Figure 4a for the device locally irradiated with 400 ions nm^{-2} , we reach dark count rates of 7 mHz and 0.55 mHz at internal detection efficiencies of 94% and 31%, respectively. Also the two regimes of intrinsic dark counts and dark counts originating from black body radiation are clearly visible: the first is given by the strongly current dependent contribution in the high current regime, while the second is the weaker current dependent contribution at lower currents [50]. The black body radiation induced dark count rate could be

further suppressed by using cold band-pass filters [51].

In Figure 4b we present the relative count rate saturation plateau width, defined as

$$\sigma_{\text{rel}} = \frac{I_c - I_{\text{sat}}}{I_c}, \quad (1)$$

with the critical current I_c , and I_{sat} representing the current where the saturation plateau begins (where the normalized count rate reaches 0.95). The critical current is defined as the smallest bias current where the SNSPD shows non-zero resistance. Since we use a shunt resistor for the CR measurements to prevent latching of the detectors, the SNSPDs transition to the relaxation oscillation regime at I_c before switching to the latching state [52]. Most importantly, the relative saturation plateau width is higher for locally irradiated SNSPDs compared to fully irradiated SNSPDs of the same He ion fluence. Furthermore, the relative saturation plateau width increases strongest as a function of He ion fluence for values smaller than 200 ions nm^{-2} and, as elaborated in the supplementary, it peaks between 600 ions nm^{-2} and 1000 ions nm^{-2} before it decreases again for higher fluences.

To assess the performance of the device locally irradiated with 800 ions nm^{-2} for optical communication in the C-band, we measured its normalized count rate for photons with a wavelength of 1550 nm and compare it in Figure 4c with its performance for 780 nm photons. For both wavelengths the detector shows saturating internal detection efficiency, even for 1550 nm where the onset of photon detection is shifted to higher bias currents due to the lower sensitivity to longer wavelength photons. Since it is the same device, the dark count rate is identical for both measurements.

Moreover, we found that the detection pulse height (relevant for assessing the requirements of the readout electronics) of locally irradiated SNSPDs is higher than that of fully irradiated SNSPDs of the same fluence, while the pulse decay time (related to the detector's dead time) is similar. These quantities are further discussed in the supplementary.

V. CONCLUSIONS

Current crowding strongly limits the maximum bias current, sensitivity, and dark count rate of SNSPDs at low temperatures. We demonstrated a method to obtain current-crowding-free SNSPDs by irradiating the straight segments of SNSPDs locally with He ions while leaving their bends unirradiated. Up to a He ion fluence of (90 ± 20) ions nm^{-2} the critical current is not reduced, meaning the photon sensitivity is enhanced without sacrificing any of the SNSPD's critical current. Above this threshold, the straight segments of the locally irradiated SNSPDs show a critical current lower than that of the bends such that current crowding in the bends does not limit the overall critical current anymore.

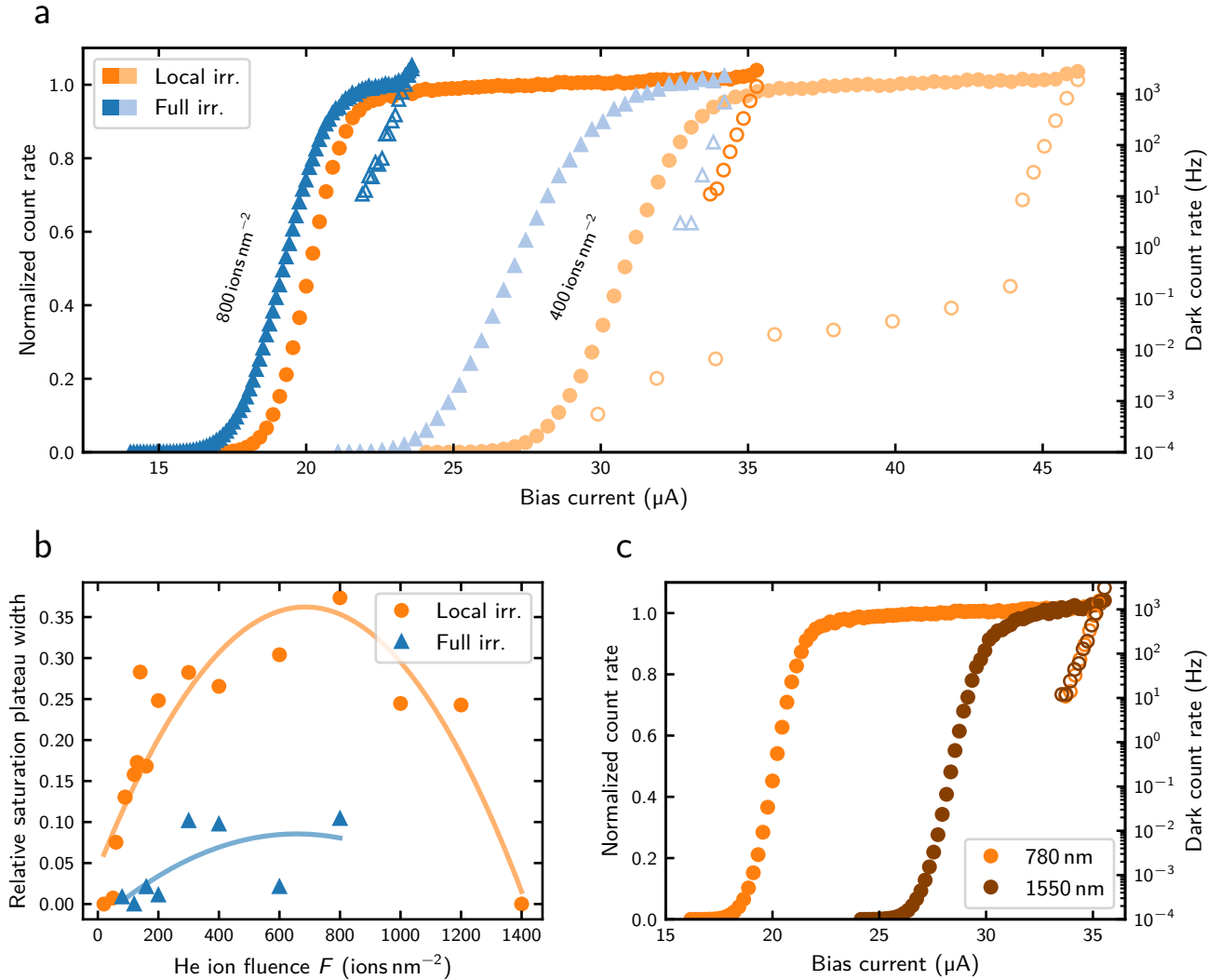


FIG. 4. Detection performance of SNSPDs after local or full irradiation with He ions. **a**, Normalized count rate (solid symbols) and dark count rate (open symbols) versus bias current after local (orange) or full (blue) irradiation with He ions. The He ion fluence used for irradiation is shown as annotations at the corresponding count rate curves. **b**, Relative saturation plateau width versus He ion fluence after local or full irradiation, calculated according to Equation (1). The solid lines serve as a guide to the eye. **c**, Comparison of the normalized count rate between photons of 780 nm and 1550 nm wavelength for a detector locally irradiated with 800 ions nm^{-2} . All shown dark count rate data was taken such that the integration time per data point was at least 10 times higher than the inverse of the measured dark count rate.

The boost in performance for locally irradiated SNSPDs is twofold: (1) the sensitivity of the SNSPD is enhanced due to He ion irradiation, and (2) the sensitivity is higher than for fully irradiated SNSPDs due to the higher available bias currents. Using this approach, we achieved a relative saturation plateau width of 37% for a locally irradiated SNSPD compared to 10% for a fully irradiated SNSPD, both irradiated with 800 ions nm^{-2} . This larger relative plateau width means that the SNSPD can be operated at lower relative bias currents with lower dark count rates and still detect single photons efficiently (e.g., 7 mHz dark count rate at an internal detection efficiency of 94%). Therefore, this method is particularly

beneficial for applications that require high detection efficiency combined with low dark count rate, such as quantum key distribution, brain imaging, and dark matter detection. Furthermore, it is ideally suited for high fill factor or micro-scale SNSPDs that are prone to current crowding, especially if the detectors require He ion irradiation anyway to become single-photon sensitive [48]. By combining site-selective [46] with local He ion irradiation, one can realize highly and homogeneously performing SNSPD arrays. Moreover, local He ion irradiation can be further used to study the effect of current crowding in different regions of superconducting devices, including SNSPDs and the influence of current crowding in their

bends onto properties such as dark count rate, detection efficiency, and switching current.

ACKNOWLEDGMENTS

We gratefully acknowledge support from the German Federal Ministry of Education and Research (BMBF) via the funding program “Photonics Research Germany” (projects MOQUA (13N14846) and MARQUAND (BN106022)) and the funding program “Quantum technologies – from basic research to market” (projects PhotonQ (13N15760), SPINNING (13N16214), QPIS (16K1SQ033), QPIC-1 (13N15855) and SEQT (13N15982)), as well as from the German Research Foundation (DFG) under Germany’s Excellence Strategy EXC-2111 (390814868) with the projects PQET (INST 95/1654-1) and MQCL (INST 95/1720-1). This research is part of the “Munich Quantum Valley”, which is supported by the Bavarian state government with funds from the “Hightech Agenda Bayern Plus”.

METHODS

A. Fabrication of NbTiN SNSPDs

To fabricate SNSPDs and straight wires, we deposited an 8 nm thick NbTiN film using DC reactive magnetron sputtering onto a Si substrate with a 130 nm thick thermally grown SiO₂ layer. The superconductor thickness was controlled by measuring the sputtering rate and choosing the sputtering time correspondingly. Subsequently, we patterned the SNSPDs and straight wires with electron beam lithography and reactive ion etching, followed by contact pad fabrication using optical lithography and gold evaporation [53]. The detector design consists of 250 nm wide nanowires in meander form

with 100 nm gaps (fill factor 71 %) and covers an active area of 20 μm × 20 μm. To have a pronounced effect of current crowding, a nominally rectangular design of the bends between neighboring nanowires of the SNSPDs was chosen. Similar to the detectors, the straight wires were designed to be 250 nm wide and fabricated on the same chip to ensure best comparability. After characterization of the unirradiated devices, we used a He ion microscope (Zeiss Orion Nanofab) for irradiation with He ions with an acceleration voltage of 30 kV. For the locally irradiated devices we chose an irradiation area of 25 μm × 15 μm, centered on the 20 μm × 20 μm detectors. Two detectors were fully irradiated with an irradiation area of 25 μm × 25 μm. For the reference straight wires, an irradiation area of 5 μm × 15 μm was chosen. After irradiation, we characterized the devices again and repeated the process of irradiation and subsequent measurements for several devices multiple times.

B. Low-temperature measurements

All detectors were pre-characterized in a cryogenic probe station (Janis) at 4.5 K. Subsequently, devices exhibiting a similar switching current of (42 ± 2) μA at 4.5 K were selected for wire bonding and further characterization at temperatures down to 150 mK in a closed cycle cryostat with adiabatic demagnetization refrigeration (kiutra GmbH). Further characterization consisted of measuring the switching current of each device 10–250 times to determine a switching current distribution and its mean switching current at a temperature of 1 K. The switching current measurements were performed by ramping the bias voltage applied at a 50 kΩ resistor in series to the respective device and determining the current at which the total resistance increases by more than 1 kΩ. Temperature dependent switching current measurements were performed at temperature ramp rates of 0.075 K/min, ensuring that during one bias voltage sweep the temperature change was less than 0.1 K.

-
- [1] G. N. Gol’tsman, O. Okunev, G. Chulkova, A. Lipatov, A. Semenov, K. Smirnov, B. Voronov, A. Dzardanov, C. Williams, and R. Sobolewski, Picosecond superconducting single-photon optical detector, *Applied Physics Letters* **79**, 705 (2001).
- [2] H. Takesue, S. W. Nam, Q. Zhang, R. H. Hadfield, T. Honjo, K. Tamaki, and Y. Yamamoto, Quantum key distribution over a 40-dB channel loss using superconducting single-photon detectors, *Nature Photonics* **1**, 343 (2007).
- [3] J.-P. Chen, C. Zhang, Y. Liu, C. Jiang, D.-F. Zhao, W.-J. Zhang, F.-X. Chen, H. Li, L.-X. You, Z. Wang, Y. Chen, X.-B. Wang, Q. Zhang, and J.-W. Pan, Quantum Key Distribution over 658 km Fiber with Distributed Vibration Sensing, *Physical Review Letters* **128**, 180502 (2022).
- [4] Y. Liu, W.-J. Zhang, C. Jiang, J.-P. Chen, C. Zhang, W.-X. Pan, D. Ma, H. Dong, J.-M. Xiong, C.-J. Zhang, H. Li, R.-C. Wang, J. Wu, T.-Y. Chen, L. You, X.-B. Wang, Q. Zhang, and J.-W. Pan, Experimental Twin-Field Quantum Key Distribution over 1000 km Fiber Distance, *Physical Review Letters* **130**, 210801 (2023).
- [5] F. Bussi eres, C. Clausen, A. Tiranov, B. Korzh, V. B. Verma, S. W. Nam, F. Marsili, A. Ferrier, P. Goldner, H. Herrmann, C. Silberhorn, W. Sohler, M. Afzelius, and N. Gisin, Quantum teleportation from a telecom-wavelength photon to a solid-state quantum memory, *Nature Photonics* **8**, 775 (2014).
- [6] H. Takesue, S. D. Dyer, M. J. Stevens, V. Verma, R. P. Mirin, and S. W. Nam, Quantum teleportation over 100 km of fiber using highly efficient superconducting nanowire single-photon detectors, *Optica* **2**, 832 (2015).

- [7] H. Shibata, T. Honjo, and K. Shimizu, Quantum key distribution over a 72 dB channel loss using ultralow dark count superconducting single-photon detectors, *Optics Letters* **39**, 5078 (2014).
- [8] R. Valivarthi, M. G. Puigibert, Q. Zhou, G. H. Aguilar, V. B. Verma, F. Marsili, M. D. Shaw, S. W. Nam, D. Oblak, and W. Tittel, Quantum teleportation across a metropolitan fibre network, *Nature Photonics* **10**, 676 (2016).
- [9] C. M. Natarajan, M. G. Tanner, and R. H. Hadfield, Superconducting nanowire single-photon detectors: Physics and applications, *Superconductor Science and Technology* **25**, 063001 (2012).
- [10] E. E. Wollman, V. B. Verma, A. B. Walter, J. Chiles, B. Korzh, J. P. Allmaras, Y. Zhai, A. E. Lita, A. N. McCaughan, E. Schmidt, S. Frasca, R. P. Mirin, S. W. Nam, and M. D. Shaw, Recent advances in superconducting nanowire single-photon detector technology for exoplanet transit spectroscopy in the mid-infrared, *Journal of Astronomical Telescopes, Instruments, and Systems* **7**, 011004 (2021).
- [11] M. E. Grein, A. J. Kerman, E. A. Dauler, M. M. Willis, B. Romkey, R. J. Molnar, B. S. Robinson, D. V. Murphy, and D. M. Boroson, An optical receiver for the Lunar Laser Communication Demonstration based on photon-counting superconducting nanowires, *Advanced Photon Counting Techniques IX* **9492**, 949208 (2015).
- [12] A. Biswas, M. Srinivasan, R. Rogalin, S. Piazzolla, J. Liu, B. Schratz, A. Wong, E. Alerstam, M. Wright, W. T. Roberts, J. Kovalik, G. Ortiz, A. Na-Nakornpanom, M. Shaw, C. Okino, K. Andrews, M. Peng, D. Orozco, and W. Klipstein, Status of NASA's deep space optical communication technology demonstration, in *2017 IEEE International Conference on Space Optical Systems and Applications (ICSOS)* (IEEE, Naha, 2017) pp. 23–27.
- [13] F. Xia, M. Gevers, A. Fognini, A. T. Mok, B. Li, N. Akbari, I. E. Zadeh, J. Qin-Dregely, and C. Xu, Short-Wave Infrared Confocal Fluorescence Imaging of Deep Mouse Brain with a Superconducting Nanowire Single-Photon Detector, *ACS Photonics* **8**, 2800 (2021).
- [14] A. Tamimi, M. Caldarola, S. Hambura, J. C. Boffi, N. Noordzij, J. W. N. Los, A. Guardiani, H. Kooiman, L. Wang, C. Kieser, F. Braun, A. Fognini, and R. Prevedel, Deep mouse brain two-photon near-infrared fluorescence imaging using a superconducting nanowire single-photon detector array (2023).
- [15] N. Ozana, A. I. Zavriyev, D. Mazumder, M. B. Robinson, K. Kaya, M. H. Blackwell, S. A. Carp, and M. A. Franceschini, Superconducting nanowire single-photon sensing of cerebral blood flow, *Neurophotonics* **8**, 035006 (2021).
- [16] F. Marsili, F. Bellei, F. Najafi, A. E. Dane, E. A. Dauler, R. J. Molnar, and K. K. Berggren, Efficient Single Photon Detection from 500nm to 5 μ m Wavelength, *Nano Letters* **12**, 4799 (2012).
- [17] A. Korneev, Yu. Korneeva, I. Florya, B. Voronov, and G. Goltsman, NbN Nanowire Superconducting Single-Photon Detector for Mid-Infrared, *Physics Procedia* **36**, 72 (2012).
- [18] H. Shibata, K. Shimizu, H. Takesue, and Y. Tokura, Ultimate low system dark-count rate for superconducting nanowire single-photon detector, *Optics Letters* **40**, 3428 (2015).
- [19] B. Korzh, Q. Y. Zhao, J. P. Allmaras, S. Frasca, T. M. Autry, E. A. Bersin, A. D. Beyer, R. M. Briggs, B. Bum- ble, M. Colangelo, G. M. Crouch, A. E. Dane, T. Gerrits, A. E. Lita, F. Marsili, G. Moody, C. Peña, E. Ramirez, J. D. Rezac, N. Sinclair, M. J. Stevens, A. E. Velasco, V. B. Verma, E. E. Wollman, S. Xie, D. Zhu, P. D. Hale, M. Spiropulu, K. L. Silverman, R. P. Mirin, S. W. Nam, A. G. Kozorezov, M. D. Shaw, and K. K. Berggren, Demonstration of sub-3 ps temporal resolution with a superconducting nanowire single-photon detector, *Nature Photonics* **14**, 250 (2020).
- [20] S. Cherednichenko, N. Acharya, E. Novoselov, and V. Drakinskiy, Low kinetic inductance superconducting MgB₂ nanowires with a 130 ps relaxation time for single-photon detection applications, *Superconductor Science and Technology* **34**, 044001 (2021).
- [21] S. Slussarenko and G. J. Pryde, Photonic quantum information processing: A concise review, *Applied Physics Reviews* **6**, 041303 (2019).
- [22] S. Gyger, J. Zichi, L. Schweickert, A. W. Elshaari, S. Steinhauer, S. F. Covre Da Silva, A. Rastelli, V. Zwiller, K. D. Jöns, and C. Errando-Herranz, Reconfigurable photonics with on-chip single-photon detectors, *Nature Communications* **12**, 1408 (2021).
- [23] S. Ferrari, C. Schuck, and W. Pernice, Waveguide-integrated superconducting nanowire single-photon detectors, *Nanophotonics* **7**, 1725 (2018).
- [24] J. P. Sprengers, A. Gaggero, D. Sahin, S. Jahanmirinejad, G. Frucci, F. Mattioli, R. Leoni, J. Beetz, M. Lerner, M. Kamp, S. Höfling, R. Sanjines, and A. Fiore, Waveguide superconducting single-photon detectors for integrated quantum photonic circuits, *Applied Physics Letters* **99**, 181110 (2011).
- [25] G. Reithmaier, S. Lichtmanecker, T. Reichert, P. Hasch, K. Müller, M. Bichler, R. Gross, and J. J. Finley, On-chip time resolved detection of quantum dot emission using integrated superconducting single photon detectors, *Scientific Reports* **3**, 1901 (2013).
- [26] G. Reithmaier, M. Kaniber, F. Flassig, S. Lichtmanecker, K. Müller, A. Andrejew, J. Vučković, R. Gross, and J. J. Finley, On-Chip Generation, Routing, and Detection of Resonance Fluorescence, *Nano Letters* **15**, 5208 (2015).
- [27] S. Majety, S. Strohauer, P. Saha, F. Wietschorke, J. J. Finley, K. Müller, and M. Radulaski, Triangular quantum photonic devices with integrated detectors in silicon carbide, *Materials for Quantum Technology* **3**, 015004 (2023).
- [28] T. Polakovic, W. Armstrong, G. Karapetrov, Z. E. Mezzani, and V. Novosad, Unconventional applications of superconducting nanowire single photon detectors, *Nanomaterials* **10**, 1198 (2020).
- [29] M. Shigefuji, A. Osada, M. Yabuno, S. Miki, H. Terai, and A. Noguchi, Efficient low-energy single-electron detection using a large-area superconducting microstrip (2023), arXiv:2301.11212 [cond-mat, physics:physics, physics:quant-ph].
- [30] Y. Hochberg, I. Charaev, S.-W. Nam, V. Verma, M. Colangelo, and K. K. Berggren, Detecting Sub-GeV Dark Matter with Superconducting Nanowires, *Physical Review Letters* **123**, 151802 (2019).
- [31] J. Chiles, I. Charaev, R. Lasenby, M. Baryakhtar, J. Huang, A. Roshko, G. Burton, M. Colangelo, K. Van Tilburg, A. Arvanitaki, S. W. Nam, and K. K. Berggren, New Constraints on Dark Photon Dark Matter with Superconducting Nanowire Detectors in an Optical

- Haloscope, *Physical Review Letters* **128**, 231802 (2022).
- [32] J. R. Clem and K. K. Berggren, Geometry-dependent critical currents in superconducting nanocircuits, *Physical Review B* **84**, 10.1103/PhysRevB.84.174510 (2011).
- [33] M. Jönsson, R. Vedin, S. Gyger, J. A. Sutton, S. Steinhauer, V. Zwiller, M. Wallin, and J. Lidmar, Current Crowding in Nanoscale Superconductors within the Ginzburg-Landau Model, *Physical Review Applied* **17**, 064046 (2022).
- [34] M. K. Akhlaghi, H. Atikian, A. Eftekharian, M. Loncar, and A. H. Majedi, Reduced dark counts in optimized geometries for superconducting nanowire single photon detectors, *Optics Express* **20**, 23610 (2012).
- [35] D. Henrich, L. Rehm, S. Dorner, M. Hofherr, K. Il'in, A. Semenov, and M. Siegel, Detection Efficiency of a Spiral-Nanowire Superconducting Single-Photon Detector, *IEEE Transactions on Applied Superconductivity* **23**, 2200405 (2013).
- [36] I. Charaev, A. Semenov, S. Doerner, G. Gomard, K. Ilin, and M. Siegel, Current dependence of the hot-spot response spectrum of superconducting single-photon detectors with different layouts, *Superconductor Science and Technology* **30**, 025016 (2017).
- [37] R. Baghdadi, E. Schmidt, S. Jahani, I. Charaev, M. G. W. Müller, M. Colangelo, D. Zhu, K. Ilin, A. D. Semenov, Z. Jacob, M. Siegel, and K. K. Berggren, Enhancing the performance of superconducting nanowire-based detectors with high-filling factor by using variable thickness, *Superconductor Science and Technology* **34**, 035010 (2021).
- [38] J.-M. Xiong, W.-J. Zhang, G.-Z. Xu, L.-X. You, X.-Y. Zhang, L. Zhang, C.-J. Zhang, D.-H. Fan, Y.-Z. Wang, H. Li, and Z. Wang, Reducing current crowding in meander superconducting strip single-photon detectors by thickening bends, *Superconductor Science and Technology* **35**, 055015 (2022).
- [39] D. Henrich, P. Reichensperger, M. Hofherr, J. M. Meckbach, K. Il'in, M. Siegel, A. Semenov, A. Zotova, and D. Yu. Vodolazov, Geometry-induced reduction of the critical current in superconducting nanowires, *Physical Review B* **86**, 144504 (2012).
- [40] H. L. Hortensius, E. F. C. Driessen, T. M. Klapwijk, K. K. Berggren, and J. R. Clem, Critical-current reduction in thin superconducting wires due to current crowding, *Applied Physics Letters* **100**, 182602 (2012).
- [41] S. Frasca, B. Korzh, M. Colangelo, D. Zhu, A. E. Lita, J. P. Allmaras, E. E. Wollman, V. B. Verma, A. E. Dane, E. Ramirez, A. D. Beyer, S. W. Nam, A. G. Kozorezov, M. D. Shaw, and K. K. Berggren, Determining the depairing current in superconducting nanowire single-photon detectors, *Physical Review B* **100**, 054520 (2019).
- [42] A. Semenov, I. Charaev, R. Lusche, K. Ilin, M. Siegel, H.-W. Hübers, N. Bralović, K. Dopf, and D. Y. Vodolazov, Asymmetry in the effect of magnetic field on photon detection and dark counts in bended nanostrips, *Physical Review B* **92**, 174518 (2015).
- [43] L. Zhang, L. You, D. Liu, W. Zhang, L. Zhang, X. Liu, J. Wu, Y. He, C. Lv, Z. Wang, and X. Xie, Characterization of superconducting nanowire single-photon detector with artificial constrictions, *AIP Advances* **4**, 067114 (2014).
- [44] X. Zhang, X. Zhang, J. Huang, C. Yang, L. You, X. Liu, P. Hu, Y. Xiao, W. Zhang, Y. Wang, L. Li, Z. Wang, and H. Li, Geometric origin of intrinsic dark counts in superconducting nanowire single-photon detectors, *Superconductivity* **1**, 100006 (2022).
- [45] W. Zhang, Q. Jia, L. You, X. Ou, H. Huang, L. Zhang, H. Li, Z. Wang, and X. Xie, Saturating Intrinsic Detection Efficiency of Superconducting Nanowire Single-Photon Detectors via Defect Engineering, *Physical Review Applied* **12**, 044040 (2019).
- [46] S. Strohauer, F. Wietschorke, L. Zugliani, R. Flaschmann, C. Schmid, S. Grotowski, M. Müller, B. Jonas, M. Althammer, R. Gross, K. Müller, and J. J. Finley, Site-Selective Enhancement of Superconducting Nanowire Single-Photon Detectors via Local Helium Ion Irradiation, *Advanced Quantum Technologies* **6**, 2300139 (2023).
- [47] M. W. Brenner, D. Roy, N. Shah, and A. Bezryadin, Dynamics of superconducting nanowires shunted with an external resistor, *Physical Review B* **85**, 224507 (2012).
- [48] I. Charaev, E. K. Batson, S. Cherednichenko, K. Reidy, V. Drakinskiy, Y. Yu, S. Lara-Avila, J. D. Thomsen, M. Colangelo, F. Incalza, K. Ilin, A. Schilling, and K. K. Berggren, Single-photon detection using large-scale high-temperature MgB₂ sensors at 20 K, *Nature Communications* **15**, 3973 (2024).
- [49] Y.-Z. Wang, W.-J. Zhang, X.-Y. Zhang, G.-Z. Xu, J.-M. Xiong, Z.-G. Chen, Y.-Y. Hong, X.-Y. Liu, P.-S. Yuan, L. Wu, Z. Wang, and L.-X. You, Free-space coupled, large-active-area superconducting microstrip single-photon detector for photon-counting time-of-flight imaging, *Applied Optics* **63**, 3130 (2024).
- [50] O. Kahl, S. Ferrari, V. Kovalyuk, G. N. Goltsman, A. Korneev, and W. H. P. Pernice, Waveguide integrated superconducting single-photon detectors with high internal quantum efficiency at telecom wavelengths, *Scientific Reports* **5**, 10941 (2015).
- [51] H. Shibata, K. Shimizu, H. Takesue, and Y. Tokura, Superconducting Nanowire Single-Photon Detector with Ultralow Dark Count Rate Using Cold Optical Filters, *Applied Physics Express* **6**, 072801 (2013).
- [52] A. J. Kerman, D. Rosenberg, R. J. Molnar, and E. A. Dauler, Readout of superconducting nanowire single-photon detectors at high count rates, *Journal of Applied Physics* **113**, 144511 (2013).
- [53] R. Flaschmann, L. Zugliani, C. Schmid, S. Spedicato, S. Strohauer, F. Wietschorke, F. Flassig, J. J. Finley, and K. Müller, The dependence of timing jitter of superconducting nanowire single-photon detectors on the multi-layer sample design and slew rate, *Nanoscale* **15**, 1086 (2023).

Supplementary: Current-Crowding-Free Superconducting Nanowire Single-Photon Detectors

Stefan Strohauer,^{1,2,*} Fabian Wietschorke,^{1,3} Christian Schmid,^{1,3} Stefanie Grotowski,^{1,2}
Lucio Zugliani,^{1,3} Björn Jonas,^{1,3} Kai Müller,^{1,3,4} and Jonathan J. Finley^{1,2,4,†}

¹Walter Schottky Institute, Technical University of Munich, 85748 Garching, Germany

²TUM School of Natural Sciences, Technical University of Munich, 85748 Garching, Germany

³TUM School of Computation, Information and Technology,
Technical University of Munich, 80333 Munich, Germany

⁴Munich Center for Quantum Science and Technology (MCQST), 80799 Munich, Germany

(Dated: July 18, 2024)

I. DETECTION PULSE CHARACTERIZATION

In this section, we analyze the recovery time and pulse height of a detection pulse after photon absorption, since both are important performance parameters of single-photon detectors.

The recovery time determines the detector's maximum count rate and can be estimated from the time constant τ_d of the exponential decay of a detection voltage pulse [1, 2]. As shown in Figure 1, the decay time of all device types increases with increasing He ion fluence in agreement with previous measurements [3]. At the same time, the decay time of locally irradiated SNSPDs follows the same curve as that of fully irradiated SNSPDs, while pulses of straight wires show a significantly faster decay due their smaller kinetic inductance. Thus, local irradiation shows no drawback with respect to the decay time compared to full irradiation of SNSPDs.

As shown in Figure 2 the pulse height of locally irradiated SNSPDs is higher than that of fully irradiated SNSPDs due to higher available bias currents after irradiating only locally. This is beneficial since higher detection voltage pulses are easier to process for the readout electronics.

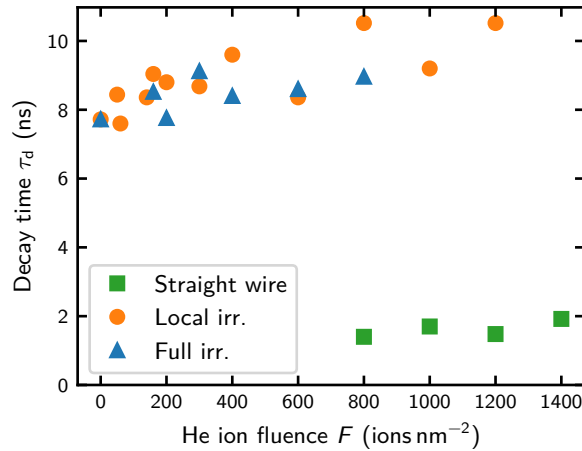


FIG. 1. Decay time versus He ion fluence for locally irradiated SNSPDs together with fully irradiated SNSPDs and straight wires as reference devices.

* stefan.strohauer@tum.de

† jj.finley@tum.de

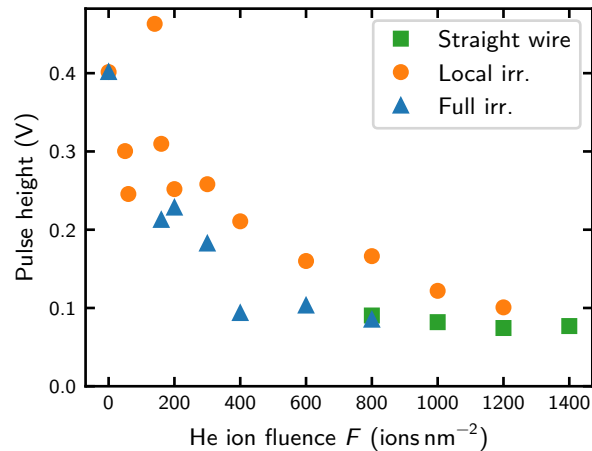


FIG. 2. Pulse height versus He ion fluence for locally irradiated SNSPDs together with fully irradiated SNSPDs and straight wires as reference devices.

II. SATURATION PLATEAU WIDTH OF LOCALLY IRRADIATED SNSPDS

The relative saturation plateau width is given by

$$\sigma_{\text{rel}} = \frac{I_c - I_{\text{sat}}}{I_c}, \quad (1)$$

with the absolute saturation plateau size given by the difference between the critical current I_c and the current I_{sat} where the saturation plateau begins. Since we use a shunt resistor for the CR measurements to prevent latching of the detectors (20.4Ω at 1 K), the SNSPDs transition to the relaxation oscillation regime at I_c before switching to the latching state. In this regime the SNSPD emits a periodic train of voltage pulses and the average voltage drop across the SNSPD increases with increasing bias current [4]. Figure 3a shows the absolute saturation plateau width $I_c - I_{\text{sat}}$ where a steep increase in saturation plateau width is observed for He ion fluences up to 200 ions nm^{-2} , followed by a decrease beyond 600 ions nm^{-2} . At the same time, the critical current decreases with increasing He ion fluence. As shown in Figure 3b, the resulting relative saturation plateau width increases for small He ion fluences, peaks between 600 ions nm^{-2} and $1000 \text{ ions nm}^{-2}$ before it decreases again for higher fluences. This relation is even better visible in Figure 3c after normalizing the saturation plateau width to the switching current of the devices without shunt resistor instead of the critical current during CR measurements.

-
- [1] S. Ferrari, C. Schuck, and W. Pernice, Waveguide-integrated superconducting nanowire single-photon detectors, *Nanophotonics* **7**, 1725 (2018).
 - [2] A. J. Kerman, E. A. Dauler, W. E. Keicher, J. K. Yang, K. K. Berggren, G. Gol'tsman, and B. Voronov, Kinetic-inductance-limited reset time of superconducting nanowire photon counters, *Applied Physics Letters* **88**, 2 (2006).
 - [3] S. Strothauer, F. Wietschorke, L. Zugliani, R. Flaschmann, C. Schmid, S. Grotowski, M. Müller, B. Jonas, M. Althammer, R. Gross, K. Müller, and J. J. Finley, Site-Selective Enhancement of Superconducting Nanowire Single-Photon Detectors via Local Helium Ion Irradiation, *Advanced Quantum Technologies* **6**, 2300139 (2023).
 - [4] A. J. Kerman, D. Rosenberg, R. J. Molnar, and E. A. Dauler, Readout of superconducting nanowire single-photon detectors at high count rates, *Journal of Applied Physics* **113**, 144511 (2013).

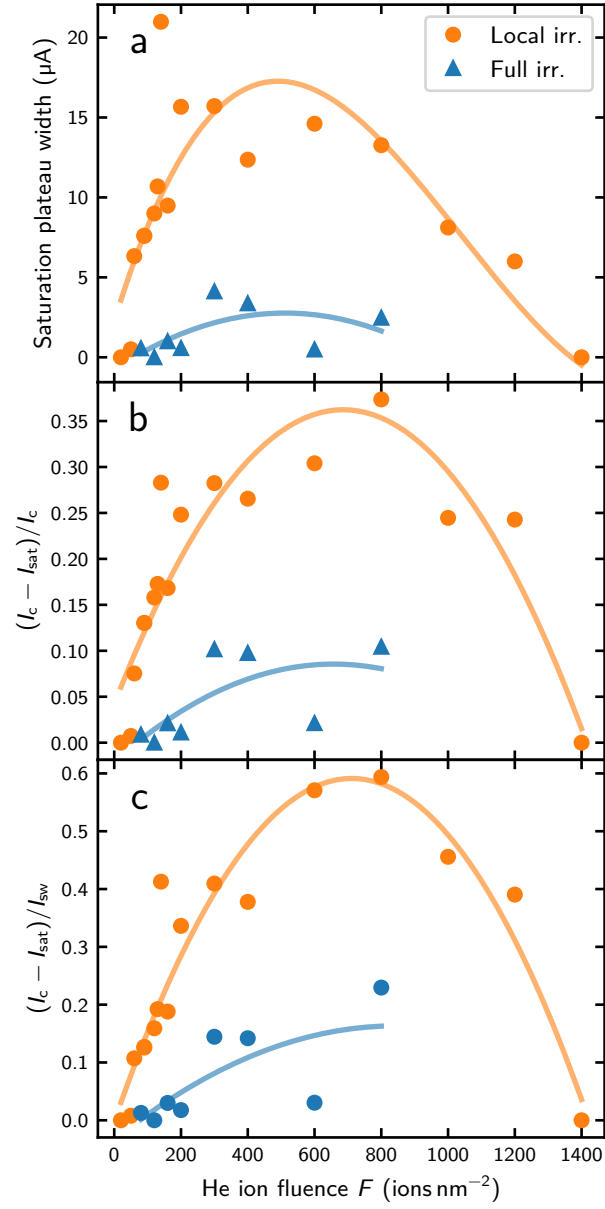


FIG. 3. Count rate saturation plateau width of locally and fully irradiated SNSPDs versus He ion fluence. **a**, Absolute saturation plateau width. **b**, Relative saturation plateau width as given in Equation (1). **c**, Saturation plateau width, normalized to the switching current of the corresponding devices measured without shunt resistor.